



This is a repository copy of *Self-consistent absorption correction for quantifying very noisy X-ray maps: group III nitride nanowires as an example.*

White Rose Research Online URL for this paper:  
<http://eprints.whiterose.ac.uk/137429/>

Version: Accepted Version

---

**Article:**

Wang, X., Bai, J. and Walther, T. [orcid.org/0000-0003-3571-6263](https://orcid.org/0000-0003-3571-6263) (2018) Self-consistent absorption correction for quantifying very noisy X-ray maps: group III nitride nanowires as an example. *Journal of Microscopy*, 272 (2). pp. 111-122. ISSN 0022-2720

<https://doi.org/10.1111/jmi.12751>

---

This is the peer reviewed version of the following article: WANG, X. , BAI, J. and WALTHER, T. (2018), Self-consistent absorption correction for quantifying very noisy X-ray maps: group III nitride nanowires as an example. *Journal of Microscopy*, 272: 111-122, which has been published in final form at <https://doi.org/10.1111/jmi.12751>. This article may be used for non-commercial purposes in accordance with Wiley Terms and Conditions for Self-Archiving.

**Reuse**

Items deposited in White Rose Research Online are protected by copyright, with all rights reserved unless indicated otherwise. They may be downloaded and/or printed for private study, or other acts as permitted by national copyright laws. The publisher or other rights holders may allow further reproduction and re-use of the full text version. This is indicated by the licence information on the White Rose Research Online record for the item.

**Takedown**

If you consider content in White Rose Research Online to be in breach of UK law, please notify us by emailing [eprints@whiterose.ac.uk](mailto:eprints@whiterose.ac.uk) including the URL of the record and the reason for the withdrawal request.



[eprints@whiterose.ac.uk](mailto:eprints@whiterose.ac.uk)  
<https://eprints.whiterose.ac.uk/>

# **Self-consistent absorption correction for quantifying very noisy X-ray maps: group III nitride nanowires as an example**

X Wang, J Bai and T Walther\*

Department of Electronic & Electrical Engineering, University of Sheffield, Mappin Street, Sheffield, S1 3JD, England, UK

\*Email: [t.walther@sheffield.ac.uk](mailto:t.walther@sheffield.ac.uk)

## **Lay Summary**

Energy-dispersive X-ray mapping in a scanning transmission electron microscope is a method to visualize the spatial distribution of chemical elements in a sample. Quantification of the signal intensities depends on proper background elimination and correction of the self-absorption of X-ray lines in the sample. Here we show that our previously developed method of self-consistent effective absorption factors works well even with extremely noisy elemental maps of a few net counts only where the human eye can hardly discern any pattern and the background signal is typically less than a single count in each spectrum channel. Correcting the background intensity to sub-pixel accuracy is then necessary for reliable quantification.

## **Abstract**

Energy-dispersive X-ray mapping in a scanning transmission electron microscope is a method to visualize the spatial distribution of chemical elements in a sample. Quantification of the signal intensities depends on proper background elimination and correction of the self-

absorption and fluorescence of X-ray lines in the sample. The latter become particularly relevant for slightly thicker and rough samples, small take-off angles and low-energetic X-ray lines, for which we have recently introduced a self-consistent absorption correction based on effective  $k^*$ -factors selected automatically from curves simulated as function of a K/L line intensity ratio of one of the heavier elements in the sample for ranges of different compositions. This has been shown to work well for thick and for rough samples. Correcting the background intensity to sub-pixel accuracy is necessary for reliable quantification of very noisy maps. In this study, we show how this self-consistent absorption correction method can be applied to InGaN and AlGaN layers in GaN nanowires, the net maps of which can be so noisy the layers can hardly be seen by the eye (a few counts per pixel) and the background is below a single count in each spectrum channel. The result indicates that background estimation for the Ga L-line intensity using fractional counts from an interpolation of maps from neighbouring X-ray lines of elements that are not actually present in the specimen is critical for quantification. The nanowires studied were between 66 nm and 375 nm thick.

## **Introduction**

For the established methods of X-ray absorption correction in analytical transmission electron microscopy (TEM) estimates of specimen thickness and density (Cliff & Lorimer, 1975), mass-thickness (August & Wernisch, 1987) or probe current (Watanabe, Horita and Nemoto, 1996) are needed. We recently developed a self-consistent absorption correction method based on effective sensitivity factors (denoted as  $k^*$ -factors) based on Monte Carlo simulations and K/L intensity ratios of at least one heavier element directly measured from the spectrum to be quantified (Walther & Wang, 2015, Walther & Wang, 2016). If maps have very low counts they are susceptible to strong shot noise and the background cannot be estimated from an integer valued map because it will be below a single count on average. In

our case of InGaN and AlGaIn layers in GaN nanowires forming radial quantum discs, the Ga L, Al K and In L X-ray lines can be strongly absorbed before they reach the detector, resulting in elemental maps with typically fewer than ten counts per pixel and hence subject to heavy shot noise. While X-ray line profiles taken along defined directions previously identified by annular dark-field imaging typically have much better counting statistics than maps with their significantly reduced pixel dwell times, the detection of unknown impurities and/or complex chemical inhomogeneities is sometimes easier and more reliable in elemental distribution maps than in any type of images. Also, strong local thickness variations can, as in the present case, be directly studied in terms of their influence on absorption correction. Furthermore, for layered structures, chemical signals from maps can easily be converted into compositional line profiles afterwards by net count summation over regions perpendicular to the corresponding interfaces, as shown in Figure 7 of this study. For our absorption correction we need the Ga K/L ratio at each pixel in the map, which will itself be not only even noisier but also suffer from quantisation effects as X-rays are detected as individual X-rays hitting the detector, so all elemental maps will have lots of zero, single and double counts. In our case these low counts are due to the low detector efficiency (with a collection solid angle of only 0.12srad, which can be increased to ~1srad in more modern set-ups with optimised silicon drift detectors (Harrach et al., 2009)), however, it will remain a principal issue in any experiments conducted with low beam current or short exposure times as necessary for beam sensitive materials or for capturing nanoparticles moving on surfaces (Walther & Mader, 1999; Boyes & Gai, 2014), so we thought it worth reporting our work-around to the problem in this case.

- i) We have acquired maps from X-ray lines by integrating the intensities over certain energy windows, both centred on the actual X-ray lines of interest as well as centred around the (hypothetical) lines of elements not actually present in the

specimen, such as S K-line and Ti K-line for InGaN, from the local averaging of which we can estimate the background for the lines of interest by linear interpolation (In L) or extrapolation (Al K below S K, Ga K above Ti K).

- ii) Outside the (Al, Ga, In)N nanowires all relevant line intensities in a map of characteristic X-ray lines should vanish: outside the InGaN quantum well the In signal and outside the AlGaN layer the Al signal should vanish, i.e. yield an average of zero. If this is not the case a few nanometres away from the nanowire where electron beam broadening is negligible, fluorescence from stray X-rays due to the supporting carbon film and/or copper grid will be responsible for this, and this background must be evaluated and subtracted.

Several groups used quantification of the In concentration of InGaN quantum wells in GaN nanowires by using the Cliff-Lorimer method (Bonef et al. 2017; Zhang et al., 2016). Tan et al. (2016) demonstrated that the apparent elemental distribution in InGaAs nanowires using EDXS elemental mapping is strongly dependent on sample geometry so they could not quantify the In distribution fully. Johannes et al. (2017) evaluated the composition of GaAs embedded in a silicon nanowire by using energy dispersive X-ray fluorescence (XRF), neglecting X-ray absorption effect in a ~190 nm thick nanowire where the absorption of soft X-ray lines (Ga L or As L) should not be neglected. For 190nm of  $\text{In}_{0.2}\text{Ga}_{0.8}\text{N}$ , for example, imaged at 200kV and analysed with a detector take-off angle of  $25^\circ$ , the Ga K/L ratio will already increase from  $R=1.24$  to 1.57, i.e., a quarter of the soft X-rays from the Ga L line would be absorbed, and the rate of change of  $\Delta R/\Delta x \approx -0.8$  would introduce further uncertainty into any absorption correction if the chemical composition,  $x$ , was not known a priori. Bender, Seidel, Favia, Richard and Vandervorst (2017) investigated X-ray absorption for quantifying the Ge distribution in a  $\text{Si}_{0.75}\text{Ge}_{0.25}$  nano-rod using four silicon drift detectors

that differed in orientation with the nanowire axis, showing nanowires often required less absorption correction than flat thin films of similar projected thickness, however, the results from the quantification of Ge K and Ge L lines were not fully consistent, which indicated the absorption correction applied to the various detectors did not quite match their model. What their study showed clearly, however, was that any absorption correction depended on the relative orientation of the X-ray detector with respect to the long axes of any needle-like nanowires. Lari et al. (2010) quantified AlGaIn nanowires by using k-factors calculated from an EDAX system, however, they only used the thin film approximation. As the nanowires in our case have hexagonal cross-section, can be quite thick and sometimes arranged in heaps that may block the direct line of sight to the X-ray detector, the thin film model is not applicable because their X-ray absorption length is different. Also, absolute measurement of X-ray absorption length in a nanowire is difficult. This clearly demonstrates that reliable absorption correction method is needed to obtain quantitative chemical information from nanowires.

## Experimental

The studied nanowires were fabricated from a commercial sapphire wafer with GaN-based thin films to produce blue light emitting diodes (LEDs) that nominally consisted of the following layers, on a corundum (0001) substrate (from bottom to top): n-GaN buffer, InGaN/GaN superlattice, InGaN multiple quantum wells (MQWs), and p-GaN top contact. A 200 nm SiO<sub>2</sub> thin film was deposited by plasma enhanced chemical vapour deposition (PECVD), followed by thermal evaporation of 10 nm nickel (Ni). The sample was then annealed at 820 °C in N<sub>2</sub> ambient for one minute, allowing the Ni thin film to transform into Ni islands. Then reactive ion etching was used to remove the free-standing SiO<sub>2</sub>. The remaining SiO<sub>2</sub> nanorods with Ni on top were finally employed as a mask to etch down to the top of the n-GaN epilayer to fabricate the GaN-based nanowires using inductively coupled plasma etching.

The nanowires were harvested for transmission electron microscopy (TEM) by breaking and scraping them off the substrate using a scalpel and dispersing them onto a holey carbon foil supported by a 200 mesh copper grid.

EDXS elemental maps were recorded in a Schottky field-emission JEOL 2010F transmission electron microscope operated at 197kV and equipped with an Oxford Instruments Si:Li detector with ultrathin polymer window. A slightly increased emission gun current of 162 μA, a large spot size and a 40 μm condenser aperture were used in STEM, yielding ~ 9.5mrad semi-angle of convergence and an electron probe just under 1nm diameter with ~1nA beam current sufficient to excite X-rays. The dwell time for single frame acquisition was 0.5ms, and for each map displayed in Figure 4 several hundred frames were added after drift correction; repeat frame numbers were N=277 (thin nanowire, Fig. 1a), 355 (medium thin nanowire, Fig. 1b) and 503 (thick nanowire, Fig. 1c), respectively. The total count rate during

X-ray acquisition on the nanowires ranged from ~250 characteristic X-ray counts/s for the thinnest to ~550 counts/s for the thickest nanowire. Three coarsely scanned elemental maps were recorded at nominal magnifications of 500kX with 128×100 pixels in size, yielding a real space sampling of 1.9nm/pixel.

## **Result and Discussion**

X-ray mapping was undertaken for three GaN based nanowires of different thicknesses. Figure 1 shows overview images of the three nanowires acquired by tilting the specimen holder so the contrast of the InGaN layers and GaN region in the annular dark field (ADF) imaging mode was maximal, which means the quantum wells appeared almost edge-on. The white rectangles in Figure 1 demonstrate the regions used for X-ray mapping.

insert Figure 1 about here

In each of the ADF images of Fig. 1 we can clearly see a multiple quantum well (MWQ) structure of 15 bright layers (InGaN) and an additional ~30nm wide dark layer of unknown origin on top. No traces of any alleged superlattices could be found.

insert Figure 2 about here

From the nanowires resting inclined on the carbon support film as shown in Figure 2, a hexagonal cross-section can be inferred; and all nanowires imaged lie on one their {1-100} side facets, the short top facets being  $\pm\{0001\}$  hexagons. If the thin carbon support is not perfectly flat but slightly sagging between the stronger and more rigid copper grid bars, then

there are two distinct possibilities of arrangement for nanowires lying flat on the carbon film, as sketched in Figure 2. For a nanowire oriented so that [0001] remains in the (x, y) plane perpendicular to the electron beam direction (shown left), the interfaces will remain edge-on; for a nanowire oriented so that [0001] is tilted out of the (x, y) plane (right side) the interfaces will no longer be edge-on and appear blurred in projection along the electron beam direction.

For both cases, the projected thickness,  $t$ , in the centre of the nanowire is directly given geometrically by  $\frac{1}{2}\sqrt{3} \approx 0.866$  times their projected widths,  $w$ . This yields the central thicknesses of the three nanowires in Figures 1 and 4 of 66nm (a), 217nm (b), and 375nm (c). Weak thickness/strain contours running in the axial directions indicate the tops of the nanowires have remained intact during harvesting, without chipping off parts.

In ADF imaging regions thicker or richer in heavy elements such as indium appear brighter (Wang, Chauvat, Ruterana & Walther, 2017), while regions thinner or where lighter elements like aluminium are enriched appear darker. Hence, in Figure 1 the multiple thin bright layers can tentatively be identified as InGa<sub>3</sub>N, the thick darker layers as AlGa<sub>3</sub>N. Between InGa<sub>3</sub>N and AlGa<sub>3</sub>N there is a region of presumably pure GaN. The sampling in the mapped regions is just sufficient to resolve the thin quantum wells, their thicknesses corresponding to 2-3 pixels only.

insert Figure 3 about here

X-ray spectra acquired with a stationary electron beam 10-20nm in diameter for two minutes each from two different regions of a nanowire are displayed on a logarithmic scale in Figure 3, together with a spectrum from the copper blank, obtained with the electron beam through the hole of the carbon support film near the copper mesh grid. The latter demonstrates very

good collimation with no spurious peaks apart from  $\text{Cu}_L$  and  $\text{Cu}_K$ . In the InGaN only, weak additional metal signals are visible due to the proximity of the iron pole piece ( $\text{Fe}_K$ ) and stray X-rays generated from the beam forming condenser aperture ( $\text{Mo}_L$  and  $\text{Mo}_K$ ), all however being at least 200 times weaker than the main characteristic  $\text{Ga}_K$  lines.

Elemental maps of the X-ray signals including background for  $\text{In}_L$ ,  $\text{Al}_K$ ,  $\text{Ga}_K$ ,  $\text{Ga}_L$  are shown in Figure 4. Also shown here are maps of  $\text{Cu}_L$  and  $\text{Ti}_K$  as examples of elements not actually present in the sample but the lines of which can be used for background estimation.

insert Figure 4 about here

For quantification, we first calculate the Ga K/L ratio for each nanowire and compare it to simulation for thin films (Walther & Wang, 2015). The Ga K/L ratio from the raw maps for the 217 nm thin nanowire is only 1.125 which is actually smaller than the minimum of 1.24 predicted for an only a few nanometres thin GaN specimen from Monte Carlo simulations (Walther & Wang, 2016). This indicates the background to the Ga L line needs to be corrected as its subtraction would increase the measured Ga K/L ratio. For the Ga K-line background correction is far less relevant, as this line is more intense and has a much lower background. Four EDXS spectra were recorded from various locations of the nanowire at different thicknesses for estimating the background contribution to the Ga L line, and are shown on a logarithmic scale in Figure 5 a). The background can be fitted by a superposition of two exponential functions which model the bremsstrahlung background and detector window efficiency, cf. Figure 5 b). The ISIS 300 software quantifies the line intensity by simply integrating the peak intensity over an energy interval a few channels wide (0.8275-1.0275 keV for  $\text{Cu}_L$  and 0.9875-1.2075 keV for  $\text{Ga}_L$ ). It is clear the Cu L and Ga L peaks overlap and part of the Cu L line contributes to the Ga L background. To evaluate the Cu L

tail contribution to the Ga L intensity, the background is subtracted from the spectrum, and each characteristic line is fitted by a Gaussian function. In the four spectra shown in Figure 5 a), each spectrum has a different Cu intensity, depending on the proximity to the copper support grid and the amount of stray X-rays generated. The ratio of fitted Ga L background to gross integrated Ga L intensity from ISIS turns out to be a linear function of the gross Cu L/Ga L ratio measured in ISIS by window summations, as shown in Figure 5 c).

insert Figure 5 about here

The total intensity in mapped regions can be calculated by adding the intensities at each pixel in the region. Then the proportion of the Ga L background intensity to be subtracted from the gross peak measurement can be obtained from Figure 5 c). The results for the three nanowires are listed in Table 1.

insert Table 1 about here

Thus, reliable background values below single counts can be obtained and subtracted from each acquired Ga<sub>L</sub> map. The In<sub>L</sub> and Al<sub>K</sub> maps are very noisy and also need to be background corrected. Here, we evaluated elemental maps of Cu<sub>L</sub>, Si<sub>K</sub>, S<sub>K</sub> and Ti<sub>K</sub>, calculated their averages and then subtracted correspondingly interpolated constants from the above maps to avoid a further increase of the noise. Then, background corrected Ga K/L ratio maps could be used to derive maps for the k\* factors as shown in Figure 6 for the 66 nm thin nanowire as an example. The evaluated In<sub>L</sub> and Al<sub>K</sub> background of the maps amounted to only 0.2 and 0.1 counts, respectively, showing the sensitivity of the technique and that simple raw outputs

from multi-channel analysers in the form of integer maps are not sufficiently accurate if the absolute count rates are very low.

insert Figure 6 about here

Figure 6 show that the maps of the indium content,  $x_{In}$ , and the aluminium content,  $y_{Al}$ , calculated from the corresponding  $k^*$ -factors for Ga L- and Ga K-lines are very similar. The InGaN quantum wells are well visible in Figures 6 d) and e), while the AlGaN layer on top is faintly visible in Figures 6 h) and i). To check quantitative consistency of the results from K- and L-lines, line profiles have been integrated perpendicular to the layers over the whole maps for 66 nm and 217 nm nanowires, while for the 375 nm thick nanowire line profiles have been integrated excluding the red triangle region in Figure 1 c) where the In L and Al K signals almost vanished in the corresponding maps of Figures 4 c) and f). The results are plotted in Figure 7.

insert Figure 7 about here

As shown in Figure 7, the values of  $x_{In}$  and  $y_{Al}$  profiles in the GaN region to the right oscillate around zero level, which indicates a satisfactory background subtraction for both  $In_L$  and  $Al_K$ . The In and Al content calculated from  $Ga_K$  and  $Ga_L$  lines give consistent results. The  $x_{In}$  profiles are sharp and clear within the noise level. As observed in Figure 7 b), the  $y_{Al}$  profile for the 66 nm thin nanowire is extremely noisy. The mean Ga K/L ratio for the 66 nm thin nanowire is  $\sim 2.5$ . This is higher than for the 217 nm thick nanowire for which it is only  $\sim 1.4$ . As observed in Figure 1 a), the investigated thin nanowire is surrounded by two much thicker nanowires towards the right and bottom left that may absorb some of the low energetic Ga L X-rays, which could lead to the sample appearing thicker in X-ray absorption correction than

it actually is. Similarly, the Al K X-ray will be strongly absorbed, thereby reducing the Al peak in the concentration profile, although this is more difficult to judge in view of the poor signal to noise ratio.

Applying the same approach to the thicker GaN nanowires, the estimated average background of  $In_L$  and  $Al_K$  for 375 nm thickness were found to be 0.72 and 0.40 counts, while for the 217 nm thick nanowire the  $In_L$  background was 0.14 counts and the  $Al_K$  background 0.15 counts. The integral  $x_{In}$  and  $y_{Al}$  profiles for both nanowires are also shown in Figure 7.

As shown in Figure 7, the  $x_{In}$  and  $y_{Al}$  profiles calculated from  $Ga_K$ ,  $Ga_L$  and  $Al_K$  for both thin and thickest nanowire are quantitatively consistent: the  $x_{In}$  profile for the 375 nm thick nanowire is similar to that of the 66 nm nanowire, with peak values in the range  $x_{In}=0.17\pm 0.02$  whereas the  $x_{In}$  profile calculated for the 217 nm thick nanowire appears broader and lower in average In concentration, which may be explained by some residual tilt of this nanowire around its short axis. The Al concentration within the AlGaIn layer for the 375 nm thick nanowire is measured as  $y_{Al}=0.23\pm 0.04$ . The  $y_{Al}$  profile for the 217 nm thick nanowire is similar to that of the 375 nm thick nanowire, yielding  $y_{Al}=0.26\pm 0.04$ , as for this much thicker layer a blur of the concentration profile due to crystal tilt is less relevant than for the much thinner quantum wells.

To accurately determine the In concentration in the quantum wells the  $x_{In}$  profile for each individual InGaIn quantum well has been fitted in Figure 8 a) with a Gaussian function for the 375 nm thick nanowire ; an average In distribution profile can then be constructed by using the mean width and integral area from each Gaussian peak. Since the full width at half maximum (FWHM) of the quantum wells was measured as 4.5-5 nm from ADF imaging in Figure 1, the scattering of the electron beam into the GaN region will lead to a decrease in the apparent In peak concentration. Therefore, the measured In concentration profiles need to be

deconvolved with the corresponding beam broadening function to get a reliable measurement of the absolute In concentration profile. As the In profile is integrated perpendicular to the growth direction, only beam broadening along the growth direction needs to be considered. Also, the beam broadening is stronger in the centre of the nanowire where it is thicker than in its side facets, therefore the In profile is mainly determined by the beam broadening function in the central region of the nanowire. The broadening of an initially 1nm wide electron beam for a 66 nm, 217 nm and 375 nm thick  $\text{In}_{0.2}\text{Ga}_{0.8}\text{N}$  nanowire has been simulated by the method developed by Walther (2004) and is shown in Figure 8 b).

insert Figure 8 about here

The absolute In distribution can be obtained by deconvolution of the averaged In profile with its corresponding beam broadening function (BBF). Such deconvolved  $x_{\text{In}}$  profiles are plotted in Figure 8 c), and the absolute In distribution profile for the 66 nm thin nanowire (maximum of  $\hat{x}_{\text{In}}=0.171$ ) is in good agreement with the In profile evaluated from the 375 nm thick nanowire (maximum  $\hat{x}_{\text{In}}=0.177$ ), while the In profile for the 217 nm nanowire appears much broader and underestimates the peak In concentration. If this nanowire lies inclined on the carbon thin film, the electron beam direction may no longer be perfectly perpendicular to the InGaN/AlGaIn interfaces, resulting in an apparently broader In profile with decreased maximum In concentration. This hypothesis has been tested by simulation of the tilt influence on In and Al distributions as demonstrated in Figures 8 d) and e).

Figure 8 e) shows that the FWHM and maximum peak concentrations of the In profiles are strongly influenced by tilting the sample over an axis with a component perpendicular to the growth direction, and the tilt angle follows a linear relationship with the FWHM of the fitted In distribution, as shown in Figure 8 f). Tilting a 217 nm thick nanowire by  $5^\circ$  perpendicular

to its long axis, the apparent FWHM of the InGaN layers increases from 5 nm to 8nm, which correlates well with the experimental observation. Compressing the FWHM of In profile from 8nm to 5nm while retaining the integral of the total amount of indium measured, the resulting rescaled profile would be in good agreement with the In concentration measured directly for the 66 nm thin and the 375 nm thick nanowires (Figure 8 g)). Therefore, the peak In concentration in the InGaN quantum wells is believed to be  $\hat{x}=0.174\pm0.014$ .

From Figure 8 c), a sample tilt of  $\sim 5^\circ$  would have negligible ( $\Delta x \leq 0.01$ ) effect on the apparent maximum concentration of the Al profile since the AlGaIn layer is much thicker than the InGaN quantum wells. This explains the consistency of the Al quantification result obtained from the 217 nm and the 375 nm thick nanowire, while the Al K signal of the thinnest nanowire is too noisy to be to be interpreted quantitatively.

Photoluminescence spectra were recorded from a wider region of the as-grown sample and from the fabricated nanowire array, and are compared in Figure 9. Both samples were illuminated with a 325 nm wavelength He-Cd laser, the emission was monochromated by a 0.5 m monochromator and recorded by a cooled silicon charge-coupled device (CCD) camera.

insert Figure 9 about here

The as-grown sample shows several characteristic peaks at energies around  $2.73\pm0.03$  eV that are presumably due to thin film interference, and a spike at 2.64eV, which is a detection artefact. The as-grown quantum wells can be assumed to be completely strained, so their In concentration can be obtained from Vegard's law for the bandgap of an InGaIn bulk alloy as reproduced in equation (1)

$$E_g(\text{In}_x\text{Ga}_{1-x}\text{N}) = x \times E_g(\text{InN}) + (1-x) \times E_g(\text{GaIn}) - bx(1-x) \quad (1)$$

where  $E_g(\text{GaN})=3.39\text{eV}$  and  $E_g(\text{InN})=0.77\text{eV}$  are the bandgaps of GaN and InN (Islam, Kaysir, Islam, Hashimoto & Yamamoto, 2013; Matsuoka, Okamoto, Nakao, Harima & Kurimoto, 2002) and  $b$  is a bowing factor which is believed to be  $b=1.32\text{eV}$  for a fully strained and  $b=2.87\text{eV}$  for a relaxed InGaN layer (Orsal et al., 2014). The In concentration correlated with the broad PL peak in the as-grown sample would then indicate values of  $x=0.175\pm 0.06$ , respectively, which correlates well with our above quantification from EDXS. The blue shift of the nanowire PL spectrum, however, cannot be explained by strain relaxation (Wang, Chauvat, Ruterana & Walther, 2017) but probably results from a reduction of the piezoelectric effect after strain relaxation (Peng, Chuang & Lou, 1999; Bochkateva et al., 2009).

## **Conclusion**

We have successfully evaluated the background effect on quantification of the In and Al content of very noisy maps of thin GaN/InGaN quantum wells embedded in GaN nanowires. Accurate background subtraction will lead to consistent results of the In and Al concentration calculated from Ga K and Ga L lines. However, for thin InGaN quantum wells, the beam broadening effect and small residual tilts of the sample will lead to a broadening of the apparent In distribution profile which can result in underestimating the maximum In concentration. To determine the correct In profile, the measured In distribution profile needs to be deconvoluted by this broadening. The result obtained after deconvolution correlated well with the In concentration measurement near the zone axis. From the PL measurement, the In concentration extracted from the optical emission spectrum agrees well with the In concentration determined from EDXS.

## References

- August H J and Wernisch J (1987) A method for determining the mass thickness of thin films using electron probe microanalysis. *Scanning* **9**, 145-155.
- Bender H, Seidel F, Favia P, Richard O and Vandervorst W (2017) X-ray absorption in pillar shaped transmission electron microscopy specimens. *Ultramicrosc.* **177**, 58-68.
- Bochkateva N I, Bogatov A L, Gorbunov R I, Latyshev F E, Zubrilov A S, Tsyuk A I, Klochkov A V, Lelikov Y S, Rebane Y T and Shreter Y G (2009) Effect of the electric field on the intensity and spectrum of emission from InGaN/GaN quantum wells. *Semiconductors.* **43** (11), 1499-1505.
- Bonef B, Catalano M, Lund C, Denbaars S P, Nakamura S, Mishra U K, Kim M J and Keller S (2017) Indium segregation in N-polar InGaN quantum wells evidenced by energy dispersive X-ray spectroscopy and atom probe tomography. *Appl. Phys. Lett.* **110**,143101.
- Boyes ED and Gai PL (2014) Aberration-corrected environmental STEM (AC ESTEM) for dynamic in-situ gas reaction studies of nanoparticle catalysts. *Proc. EMAG2013, York.* *J. Phys. Conf. Ser.* **522**, 012004.
- Cliff G and Lorimer G W (1975) The quantitative analysis of thin specimens. *J. Microsc.* **103**, 203-207.
- Harrach H, Dona P, Freitag B, Soltau H, Niculae A and Rohde M (2009), An integrated silicon drift detector system for FEI Schottky field emission transmission electron microscopes. *Microsc. & Microanal.* **15**, 208-209.

- Islam M R, Kaysir M R, Islam M J, Hashimoto A, and Yamamoto A (2013) MOVPE growth of  $\text{In}_x\text{Ga}_{1-x}\text{N}$  ( $x \approx 0.4$ ) and fabrication of homo-junction solar cells. *J. Mater. Sci. Technol.* **29**(2), 128-136.
- Johannes A, Salomon D, Martinez-Criado G, Glaser M, Lugstein A and Ronning C (2017) In operando x-ray imaging of nanoscale devices: Composition, valence and internal electrical fields. *Sci. Adv.* **3**, eaao4044.
- Lari L, Walther T, Black K, Murray R T, Bullough T J, Chalker P R, Cheze C, Geelhaar L and Riechert H (2010) GaN, AlGaN,  $\text{HfO}_2$  based radial heterostructure nanowire. *J. Phys. Conf. Ser.* **209**, 012011.
- Matsuoka T, Okamoto H, Nakao M, Harima H and Kurimoto E (2002) Optical bandgap energy of wurtzite InN. *Appl. Phys. Lett.* **81**, 1246-1248.
- Orsal G, El Gmili Y, Fressengeas N, Streque J, Djerboub R, Moudakir T, Sundaram S, Ougazzaden A and Salvestrini J P (2014) Bandgap energy bowing parameter of strained and relaxed InGaN layers. *Opt. Mat. Exp.* **4**(5), 1030-104.
- Peng L H, Chuang C W and Lou L H (1999) Piezoelectric effects in the optical properties of strained InGaN quantum wells. *Appl. Phys. Lett.* **74**(6), 795-797.
- Tan H, Fan C, Ma L, Zhang X, Fan P, Yang Y, Hu W, Zhou H, Zhuang X, Zhu X and Pan A (2016) Single-crystal InGaAs nanowire for room-temperature high-performance near-infrared photodetectors. *Nano-Micro. Lett.* **8** (1), 29-35.
- Walther T (2004) Development of a new analytical electron microscopy technique to quantify the chemistry of planar defects and to measure accurately solute segregation to grain boundaries. *J. Microsc.* **215**, 191-202.

- Walther T and Mader W (1999) Investigation of gold nano-particles by energy-filtered imaging. Proc. EMAG99, Sheffield. Inst. Phys. Conf. Ser. **161**, 243-248.
- Walther T and Wang X (2015) Self-consistent absorption correction for quantitative energy-dispersive X-ray spectroscopy of InGaN layers in analytical transmission electron microscopy. Proc. EMAG 2015, Manchester. J. Phys. Conf. Ser. **644**, 012006.
- Walther T and Wang X (2016) Self-consistent method for quantifying indium content from X-ray spectra of thick compound semiconductor specimens in a transmission electron microscope. J. Microsc. **262**(2),151-156.
- Wang X, Chauvat M P, Ruterana P and Walther T (2017) Effective absorption correction for energy dispersive X-ray spectroscopy in a scanning transmission electron microscope: analyzing the indium distribution in rough samples of InGaN alloy layers. J. Microsc. **268**, 248-253.
- Watanabe M, Horita Z and Nemoto M (1996) Absorption correction and thickness determination using  $\zeta$ -factor in quantitative X-ray microanalysis. Ultramicrosc. **65**, 187–198.
- Zhang X, Belloeil M, Jouneau P H, Bougerol C, Gayral B and Daudin B (2016) Chemical composition fluctuations and strain relaxation in InGaN nanowires: the role of the metal/nitrogen flux ratio. Material Science in Semiconductor Processing. **55**, 79-84

**Table**

nanowire thickness (nm)	Cu L intensity	Ga L intensity	Ga L background of windowing gross Ga L intensity from ISIS
66	1858	21886	0.18481
217	5132	59937	0.18612
375	18463	232040	0.17523

**Table 1:** evaluated Cu L, Ga L intensities and relative Ga L background for the three nanowires

## Figures

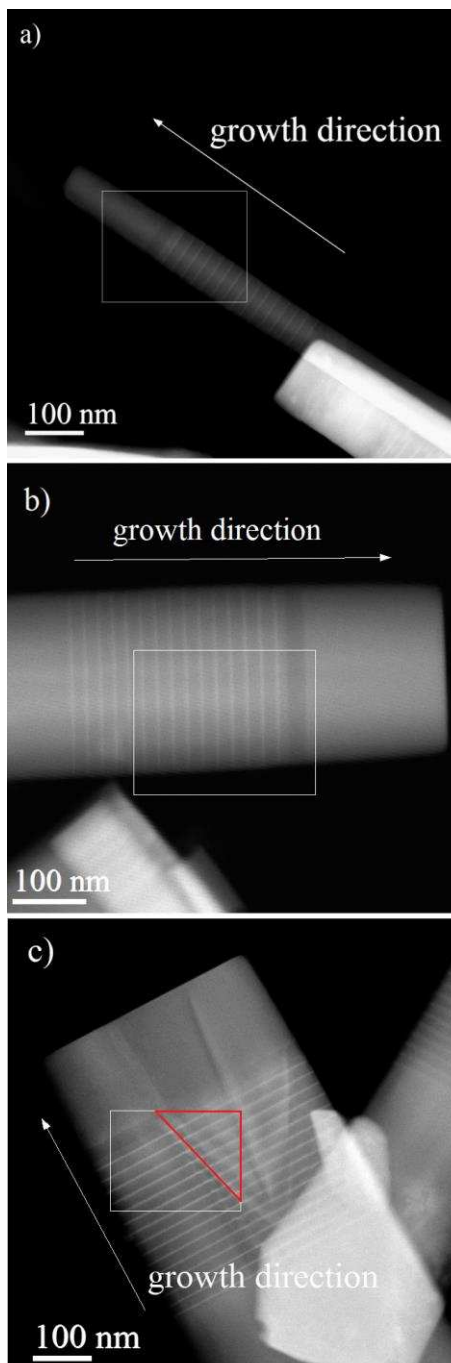


**Figure 1:** Annular dark-field (ADF) images (35-170mrad collection angle, 0.7 nm/pixel sampling) of three GaN nanowires with 15 embedded InGaN quantum wells and single AlGaN layers. Their projected widths are: a) 78 nm, b) 265 nm and c) 433 nm. The region marked by the red triangle in (c) is part of a V-pit shaped defect in the original wafer and has been excluded from the profiles in Figures 7 & 8.

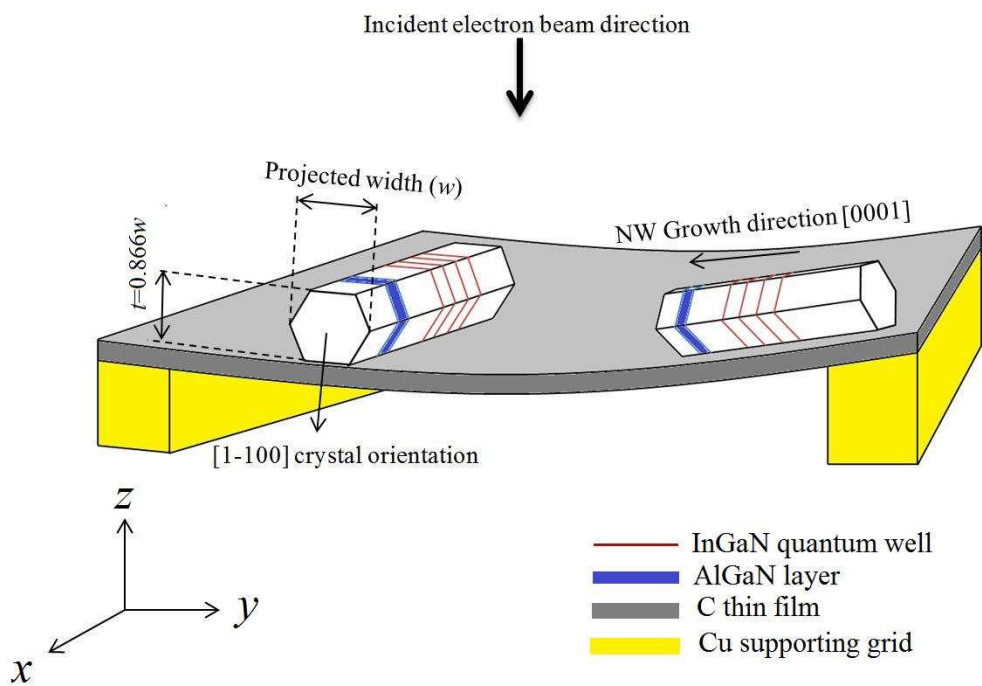


**Figure 2:** sketch of hexagonal nanowires resting on the support film.

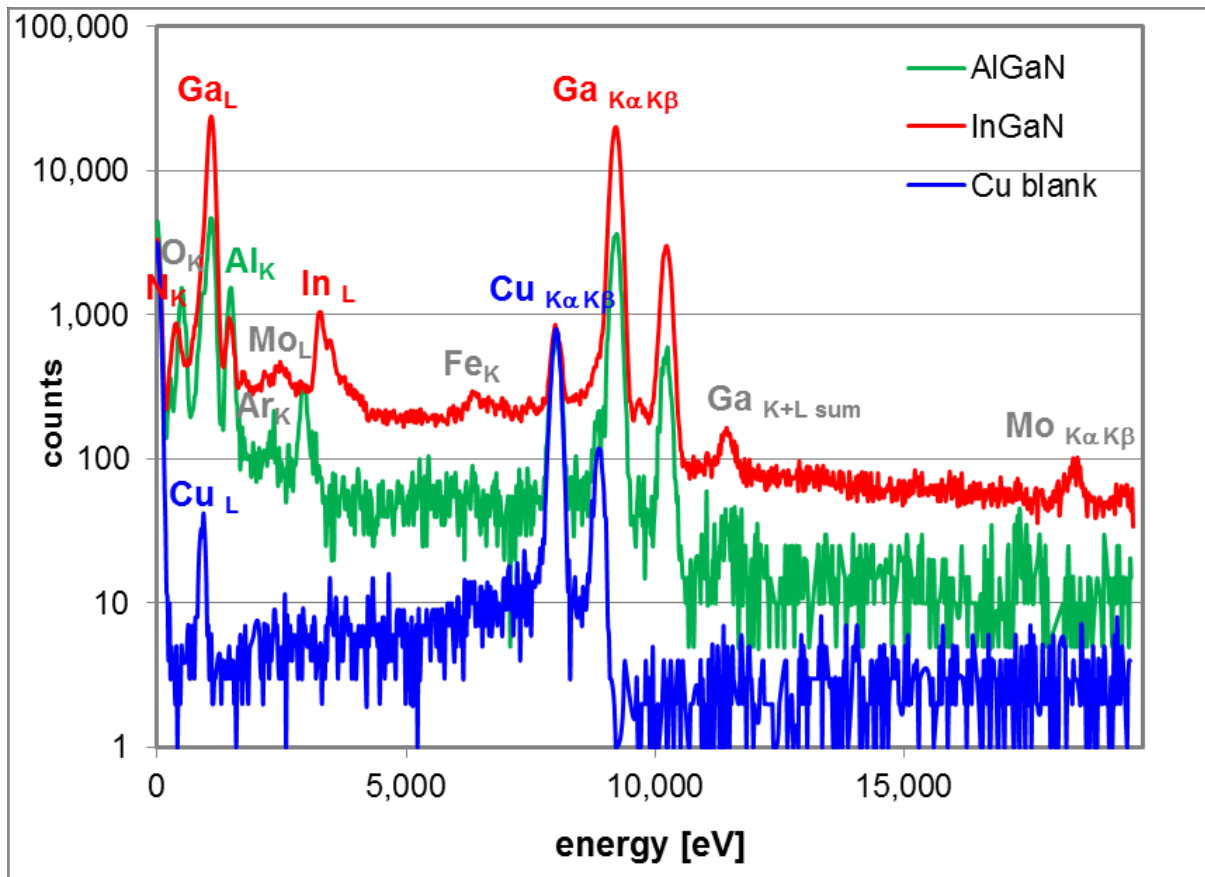


**Figure 3:** X-ray spectra recorded for 2 minutes from medium thin nanowire near position of  $\text{Al}_y\text{Ga}_{1-y}\text{N}$  layer ( $x_{\text{In}}=0.008$ ,  $y_{\text{Al}}=0.321$ , green) and  $\text{In}_x\text{Ga}_{1-x}\text{N}$  ( $x_{\text{In}}=0.033$ ,  $y_{\text{Al}}=0.034$ , red) quantum wells and from copper blank.

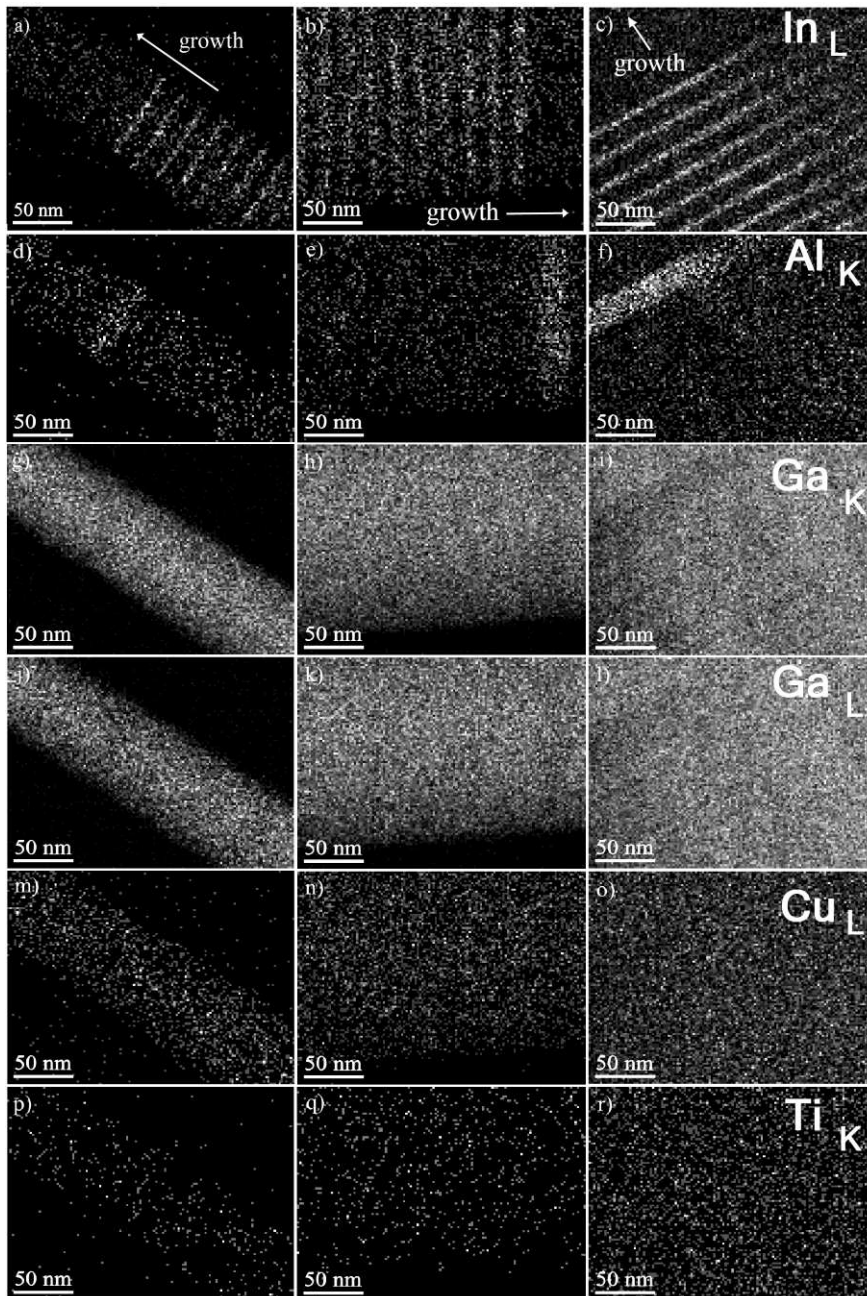


**Figure 4:** Groups of X-ray maps from nanowires: 66 nm thin (left column), 217 nm thick (middle column) and 375 nm thick nanowire (right column), top row:  $\text{In}_L$  with maximum intensities of  $\text{max}_{66\text{nm}}=4$  (a),  $\text{max}_{217\text{nm}}=6$  (b),  $\text{max}_{375\text{nm}}=13$  (c) counts, second row:  $\text{Al}_K$  with  $\text{max}_{66\text{nm}}=2$  (d),  $\text{max}_{217\text{nm}}=5$  (e),  $\text{max}_{375\text{nm}}=7$  (f), third row:  $\text{Ga}_K$  with  $\text{max}_{66\text{nm}}=17$  (g),  $\text{max}_{217\text{nm}}=18$  (h),  $\text{max}_{375\text{nm}}=42$  (i), fourth row:  $\text{Ga}_L$  with  $\text{max}_{66\text{nm}}=14$  (j),  $\text{max}_{217\text{nm}}=16$  (k),  $\text{max}_{375\text{nm}}=35$  (l), fifth row:  $\text{Cu}_L$  with  $\text{max}_{66\text{nm}}=3$  (m),  $\text{max}_{217\text{nm}}=5$  (n),  $\text{max}_{375\text{nm}}=9$  (o), sixth row:  $\text{Ti}_K$  with  $\text{max}_{66\text{nm}}=2$  (p),  $\text{max}_{217\text{nm}}=3$  (q),  $\text{max}_{375\text{nm}}=5$  (r). Min=0 for all maps.

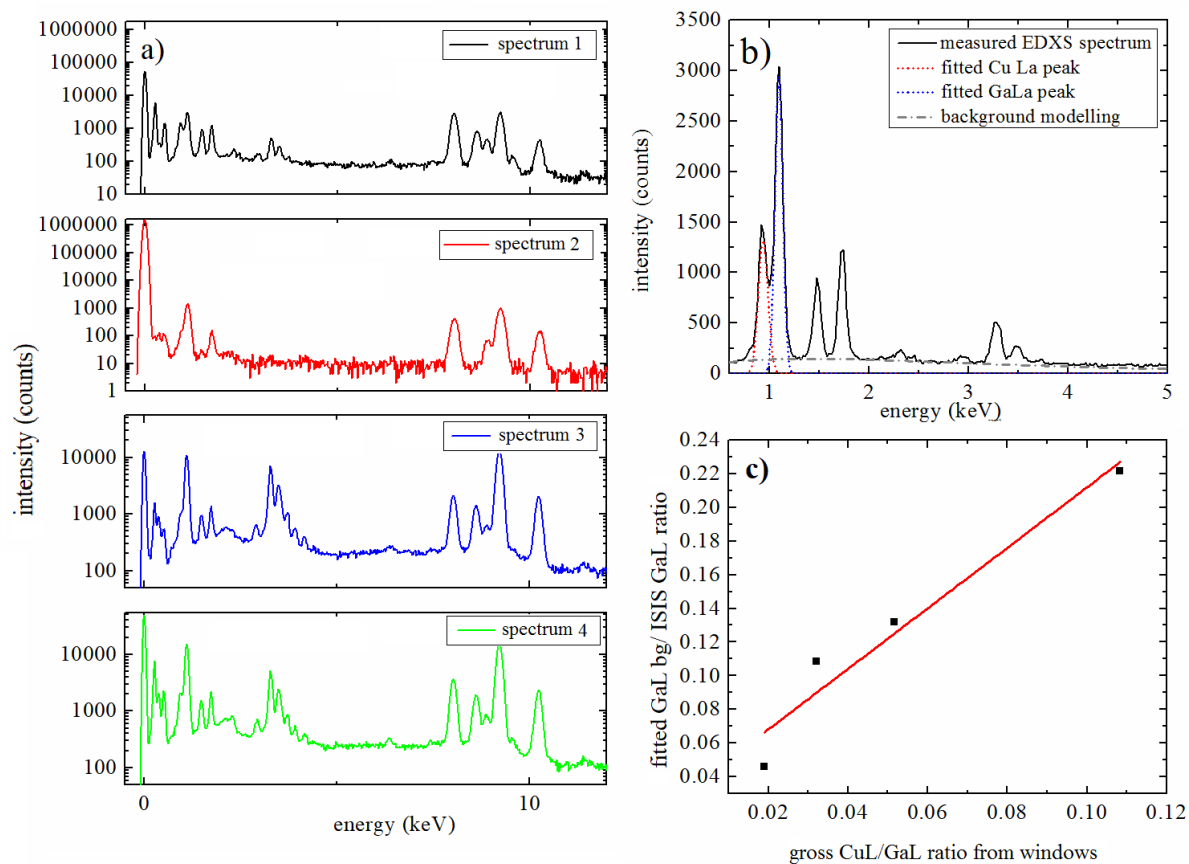


**Figure 5:** a) four X-ray spectra from (In)GaN nanowires of different thicknesses and locations on Cu support grid, displayed on logarithmic scale, b) modelled background intensity and fit of Cu L and Ga L lines by Gaussian functions, c) linear relationship between relative Ga L background under Ga L line and ISIS Cu L/Ga L ratio (window integrals).

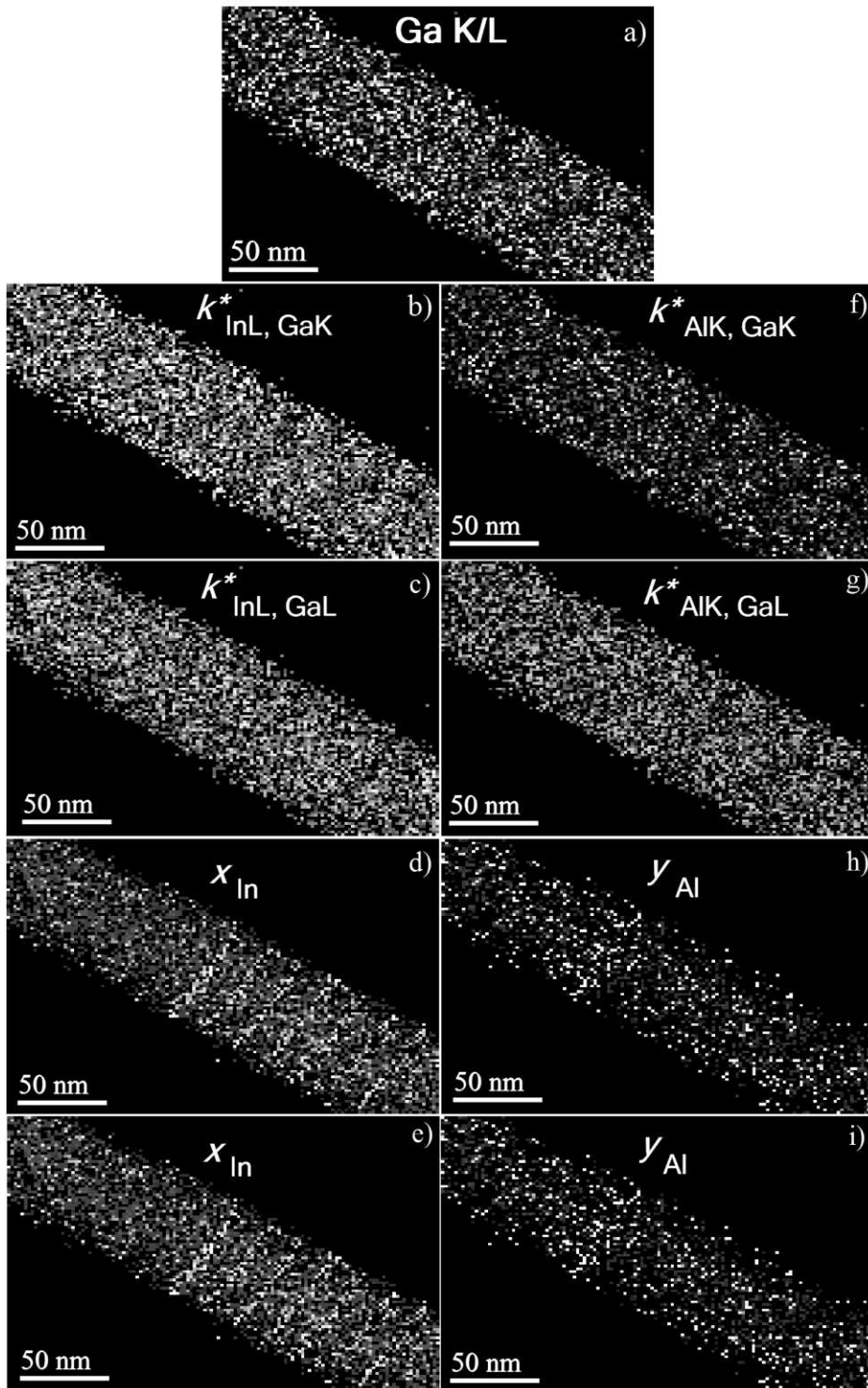


**Figure 6:** maps for the 66 nm thin  $\text{In}_x\text{Al}_y\text{Ga}_{1-x-y}\text{N}$  nanowire of a) Ga K/L ratio after optimal background correction (min=0, max=3.36), b)  $k^*_{\text{InL, GaK}}$ , c)  $k^*_{\text{InL, GaL}}$  d)  $x_{\text{In}}$  calculated from  $\text{Ga}_K$ , e)  $x_{\text{In}}$  calculated from  $\text{Ga}_L$ , f)  $k^*_{\text{AlK, GaK}}$ , g)  $k^*_{\text{AlK, GaL}}$ , h)  $y_{\text{Al}}$  calculated from  $\text{Ga}_K$ , i)  $y_{\text{Al}}$  calculated from  $\text{Ga}_L$ .

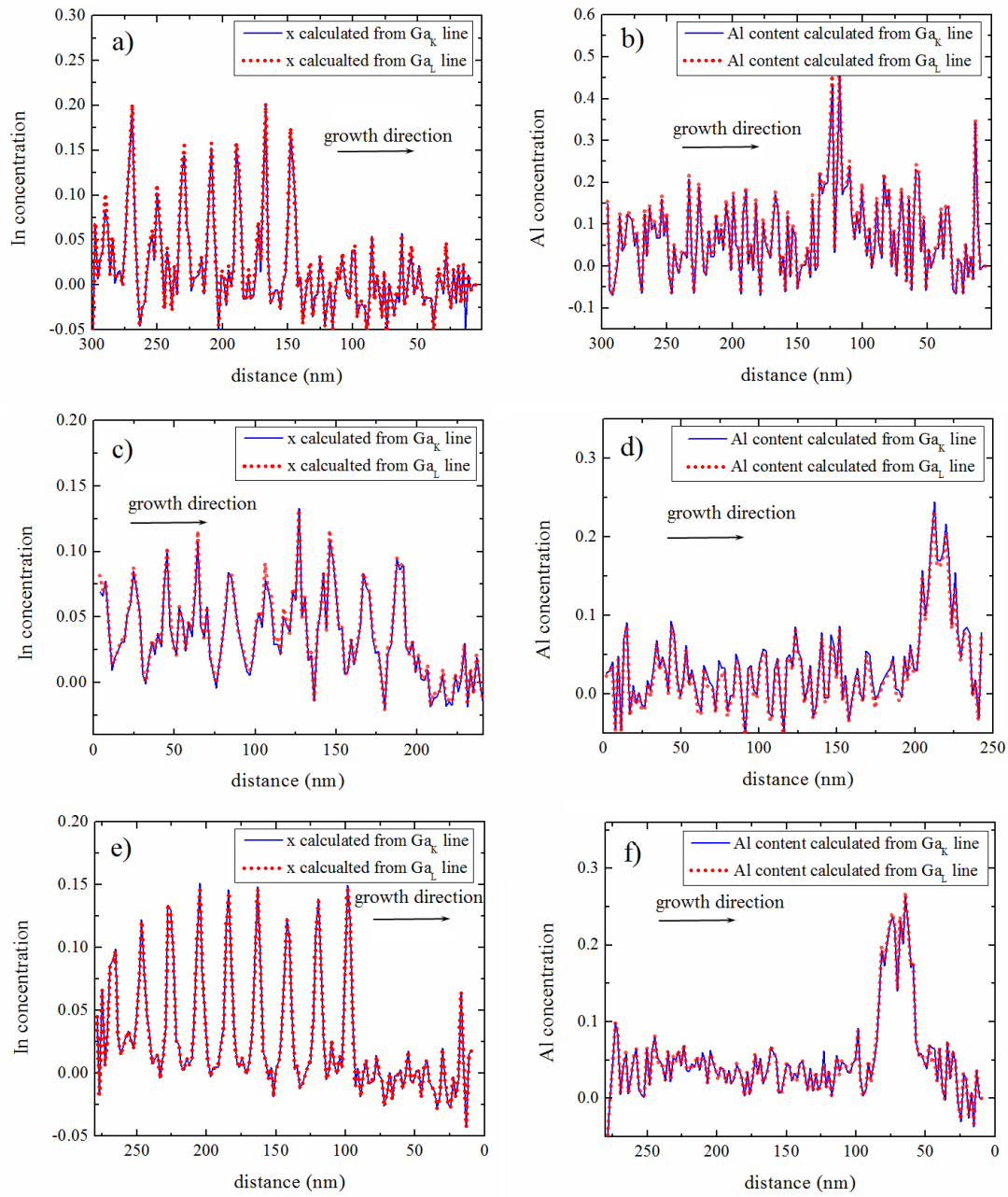


**Figure 7:** profile of  $x_{In}$  (left column) and  $y_{Al}$  (right column) calculated from  $Ga_K$  (blue lines) and  $Ga_L$  (red dots) for 66 nm thin nanowire (top row), 217 nm thick nanowire (middle row) and 375 nm thick nanowire (bottom row).

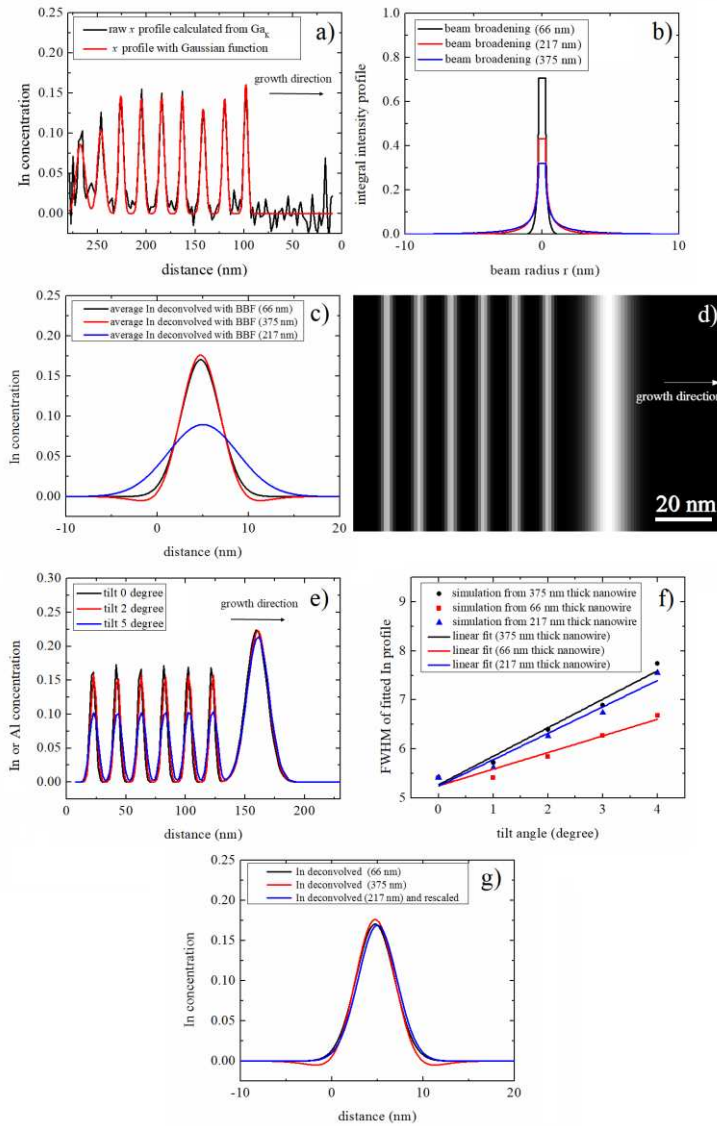


**Figure 8:** a) In profile from 375 nm thick nanowire with Gaussian fits, b) normalized beam profile of a 1nm probe after beam broadening due to multiple electron scattering in 66 nm, 217 nm and 375 nm thick  $\text{In}_{0.2}\text{Ga}_{0.8}\text{N}$ , c) average In profiles deconvolved with the corresponding beam broadening function, d) simulation of In/Al concentration profile of InGaN quantum well and AlGaIn layer, e) effect of tilt over an axis perpendicular to the growth direction on the In/Al concentration profile, f) tilt angle versus FWHM of the averaged In profile, g) comparison of averaged In profiles after deconvolution for all three nanowires and rescaling of the profile for the 217 nm fitted nanowire to same FWHM, retaining the integral.

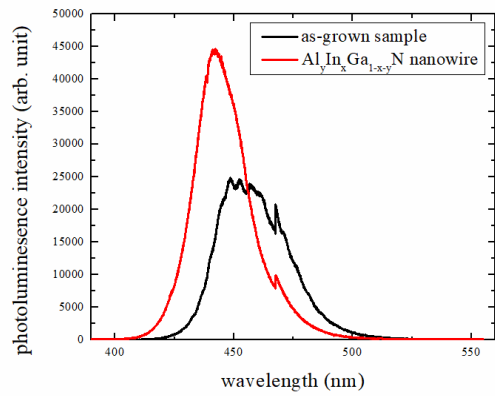


**Figure 9:** PL spectrum from the as-grown GaN/InGaN multiple quantum wells (black line) and of processed nanowire array with embedded InGaN and AlGaN layers (red line).